International Atomic Energy Agency

INDC(CCP)-385
Distrib.: G

INDC INTERNATIONAL NUCLEAR DATA COMMITTEE

Cross-Section Data Library MENDL-2 to Study Activation and Transmutation of Materials Irradiated by Nucleons of Intermediate Energies

Yu.N. Shubin, V.P. Lunev, A.Yu. Konobeyev[1], A.I. Dityuk

Institute of Physics and Power Engineering (IPPE), 249020 Obninsk, Russia

[1]Institute of Nuclear Power Engineering (INPE), 249020 Obninsk, Russia

May 1995

INDC(CCP)-385
Distrib.: G

Cross-Section Data Library MENDL-2 to Study Activation and Transmutation of Materials Irradiated by Nucleons of Intermediate Energies

Yu.N. Shubin, V.P. Lunev, A.Yu. Konobeyev[1], A.I. Dityuk

Institute of Physics and Power Engineering (IPPE), 249020 Obninsk, Russia

[1]Institute of Nuclear Power Engineering (INPE), 249020 Obninsk, Russia

Abstract

The Medium Enegy Nuclear Data Library, MENDL, contains activation cross sections for nucleons with energies up to 100 MeV incident on stable and unstable nuclei. The library is obtained by nuclear reaction model calculations using the modified version of the code ALICE-92. The present report describes physical basis and theoretical methods used to calculate reaction cross sections. Details are provided for precompound emission of nucleons, α-particles and deuterons, for nuclear level densities, equilibrium γ emission and optical model parameters. Calculated cross sections are partly corrected using available experimental data and cross-section systematics. Illustrative comparisons with experimental data for neutron and partly also for proton induced reactions are made. The MENDL data format and index are briefly described.

May 1995

CROSS-SECTION DATA LIBRARY MENDL-2 TO STUDY ACTIVATION AND TRANSMUTATION OF MATERIALS IRRADIATED BY NUCLEONS OF INTERMEDIATE ENERGIES

Yu.N.Shubin, V.P.Lunev, A.Yu.Konobeyev[1], A.I.Dityuk

Institute of Physics and Power Engineering (IPPE), 249020 Obninsk, Russia

[1]Institute of Nuclear Power Engineering (INPE), 249020 Obninsk, Russia

Nowadays the need of intermediate energy cross-section data is growing. The knowledge of these cross-sections is necessary to study activation and transmutation of materials irradiated by hard neutron spectrum of thermonuclear installations, neutron generators and accelerators. It is also important for investigation of processes taking place in irradiation of long-lived radioactive waste by intensive high energy particle fluxes.

Neutron induced reaction cross-sections at energy below 20 MeV for stable and long-lived unstable nuclei are contained in elaborated and widly used libraries REAC [1], EAF [2] and ADL-3 [3] including more than ten thousand excitation functions.

The need of analogous nuclear data for nucleons of intermediate energy ($E < 100$ MeV) were still not satisfied.

To satisfy the needs of intermediate nuclear data the cross-section library MENDL has been elaborated. MENDL (Medium Energy Nuclear Data Library) contains cross-sections for stable and unstable nuclei at energies up to 100 MeV. The first version of the library has been described in Ref.[4]. To create new version of library MENDL-2 the modified ALICE-92 code has been used. This code includes description of precompound deuteron and α-emission, the effect of nucleon and γ-competition in decay of compound nucleus and calculation of nuclear level density on the basis of generalized superfluid model.

The brief description of elaborated data library is presented below . The method of cross-section evaluation and calculation is discussed. The description of data format and library catalogue is given also.

1. Content of data library MENDL

The MENDL includes obtained by authors more than 32.000 threshold reactions taking place in neutron irradiation of nuclei from Al to Po at energies 0-100 MeV.

The data are presented in MENDL for 505 stable nuclei and unstable nuclei with half-life $T_{1/2} \geq 1$ day.

The description and fragment of MENDL catalogue are given in part 3.

2. Method to obtain cross-sections

The neutron data contained in MENDL-2 have been obtained with the help of theoretical calculations on the basis of geometry dependent hybrid exciton model and

Weisskopf evaporation model. The nuclear level density has been calculated in the framework of the superfluid nuclear model.

For some reaction channels the calculated cross-section values were corrected to achieve the agreement with available experimental data.

2.1 Cross-section calculation

2.1.1 Precompound nucleon emission

To obtain preequilibrium nucleon spectra the geometry dependent hybrid exciton model (GDH) has been used [5,6]. Calculations have been performed with help of the formula

$$\frac{d\sigma^{pre}}{d\varepsilon_x} = \pi\lambda^2 \sum_{l=0}^{\infty}(2l+1)T_l \sum_{n=n_0}^{\bar{n}} R_x(n) \cdot \frac{\omega(p-1,h,E-Q_x-\varepsilon_x)}{\omega(p,h,E)} \cdot \frac{\lambda_c^x}{\lambda_c^x+\lambda_+^x} \cdot g \cdot D_n, \qquad (1)$$

where λ is the reduced wavelength of incident particle, T_l - is the transmission coefficients calculated using optical model (see part 2.1.7), ε_x - is the energy of nucleon emitted, Q_x is the binding energy of nucleon in compound nucleus, $\omega(p,h,E)$ - is the density of n-exciton states having p particles and h holes (p+h=n) at the excitation energy E, λ_c^x - is the emission rate of nucleon, λ_+^x - is the intranuclear transition rate corresponding to absorption of nucleon in nucleus, $g = A/14.0$ - is the single particle level density, $R_x(n)$ is the number of x-particles in n-exciton state, D_n is the "depletion" factor for n-exciton state, n_0 - is the initial exciton number ($n_0 = 3$).

The density of exciton states has been calculated with help of Strutinski-Ericson formula

$$\omega(p,h,E) = \frac{g(gE-A)^{n-1}}{p!\,h!\,(n-1)!}, \qquad (2)$$

were A is the correction term for the Pauli principle equal to $A = (p^2+h^2+p-3h)/4$.

To calculate the emission rate of nucleon the following relation has been used

$$\lambda_c^x = \frac{(2s_x+1)\mu_x\varepsilon_x\sigma_{inv}^x(\varepsilon_x)}{\pi^2\hbar^3 g_x}, \qquad (3)$$

were s_x and μ_x - are spin and reduced mass for particle of x-type, σ^x_{inv} - is the inverse reaction cross-section for considered particle, g_x is the single level density for x-particle which equal to $g_n = N/14.0$ for neutrons and $g_p = Z/14.0$ for protons.

The intranuclear transition rate has been calculated by the following formula

$$\lambda_+^x = V\sigma_0(\varepsilon_x)\rho_l \qquad (4)$$

were V is the velocity of nucleon moving inside the nucleus, σ_0 - is the Pauli principle corrected cross-section of nucleon-nucleon interactions [7], ρ_l - is the nuclear density. In initial state (2p1h) for each partial wave ρ_l has been calculated by averaging of nuclear density in the range $l\lambda < r < (l+1)\lambda$. For other exciton states the nuclear density has been averaged over nucleus volume.

The factor $R_X(n)$ included in formula (1) was calculated for neutron induced reactions by the following way

$$R_n(3) = (Z + 2A)/(2Z + A) \qquad (5a)$$

$$R_p(n) = 2 - R_x(3) \qquad (5b)$$

$$R_x(n) = R_x(3)+(n-3)/4 \qquad (5c)$$

The calculation of nonequilibrium spectra was carried out approximately taking into account multiple precompound nucleon emission. According to [6] it was assumed that the number of particles emitted from a particular exciton state is equal to

$$P_{np} = P_n P_p \qquad \text{(for emission of neutron and proton)} \qquad (6a)$$

$$P_{nn} = P_n P_{\bar{n}}/2 \qquad \text{(for emission of two neutrons)} \qquad (6b)$$

here P_n and P_p are total numbers of neutrons and protons emitted from considered n-exciton configuration.

The precompound components of spectrum for (n,n'), (n,2n) and (n,np) reactions were calculated by following formulae

$$\sigma^{Z,A}(E_n-\varepsilon)=\frac{C_n}{\sigma_n}\cdot\frac{d\sigma_n(\varepsilon)}{d\varepsilon}, \qquad (7a)$$

$$\sigma^{Z,A-1}(E_n+Q_{(n,2n)}-\varepsilon-\bar{\varepsilon}_n)=\frac{C_{nn}/2}{\sigma_{2n}}\cdot\frac{d\sigma_n(\varepsilon)}{d\varepsilon}, \qquad (7b)$$

$$\sigma^{Z-1,A-1}(E_n+Q_{(n,np)}-\varepsilon-\bar{\varepsilon}_{p(n)})=\frac{C_{np}}{2\sigma_{np}}\left[\frac{d\sigma_n(\varepsilon)}{d\varepsilon}\right]\left(1-V_p/\varepsilon\right)+\frac{C_{np}}{2\sigma_{pn}}\left[\frac{d\sigma_p(\varepsilon)}{d\varepsilon}\right], \qquad (7c)$$

where Z, A are characteristics of target nucleus, E_n is the energy of incident neutrons, Q_n and $Q_{(n,np)}$ are (n,2n) and (n,np) reaction energies, V_p is the proton Coulomb potential, C_n, C_{nn} and C_{np} are, correspondingly, the cross-section of emission of single precompound neutron, the cross-section of coincident emission of two precompound neutrons from the same exciton states and the cross-section of neutron and proton emission in coincidence from these states, σ_n and σ_{2n} are energy integrated total preequilibrium spectra of neutrons ($d\sigma_n/d\varepsilon$) in the energy ranges corresponding to (n,n') reaction ($E-B_n$) and (n,2n) reaction ($E-B_{2n}$), σ_{np} and σ_{pn} are energy integrated total preequilibrium spectra of neutrons ($d\sigma_n/d\varepsilon$) and protons ($d\sigma_p/d\varepsilon$) in the energy range from 0 to $E_n+Q_{(n.np)}$, $\bar{\varepsilon}_n$ and $\bar{\varepsilon}_p$ - are average kinetic energies of neutron and proton corresponding to the kinetic energy ε of the first emitted particle.

2.1.2 Precompound α-emission

To obtain nonequilibrium α-particle spectra the coalescence pick-up model [8,9] combined with hybrid exciton model has been used. The calculations has been performed with help of the formula:

$$\frac{d\sigma^{pre}}{d\varepsilon_x} = \sigma_{non} \sum_{l+m=4} \sum_{n} F_{l,m}(\varepsilon_\alpha) \cdot \frac{\omega(p-l,h,E-Q_\alpha-\varepsilon_\alpha)}{\omega(p,h,E)} \cdot \frac{\lambda_c^\alpha}{\lambda_c^\alpha+\lambda_+^\alpha} \cdot g_\alpha \cdot D_n, \qquad (8)$$

where σ_{non} is the nonelastic reaction cross-section, $F_{l,m}(\varepsilon_\alpha)$ is the probability of α-particle formation from l excited and m nonexcited quasiparticles in the nucleus [8], g_α is the single α-particle level density.

The emission rate of α-particle was calculated by the following way

$$\lambda_c^x = \frac{\mu_\alpha \varepsilon_\alpha \sigma_{inv}^\alpha(\varepsilon_\alpha)}{\pi^2 \hbar^3 g_\alpha}, \qquad (9)$$

The intranuclear transition rate λ^α_+ characterizing the absorption of the excited α-particle in the nucleus was calculated using relation:

$$\lambda_+^\alpha = 2W_{opt}^\alpha/\hbar\ , \qquad (10)$$

where W^α_{opt} is the imaginary part of the optical potential for α-particles interacting with nuclei. In the present calculations the value of $\sum_{l+m=4} F_{l,m}$ for all nuclei was chosen from comparison with experimental data and was taken to be equal to 0.41.

As an illustration the cross-sections calculated using considered approach to describe nonequilibrium α-particle emission are shown in Fig.1. The example of the α-particle spectrum calculation is presented in Fig.1 for ^{120}Sn(p,α)x reaction at the incident proton energy 62 MeV. The calculated excitation functions for reaction with α-particle emission are shown for ^{98}Mo, ^{197}Au and ^{202}Hg also. The contribution of equilibrium α-emission is illustrated in Fig.1. For ^{197}Au(n,α) reaction this

contribution is actually equal to zero. As seen from figure the calculation without taken into account the precompound α-emission is not described the experimental cross-section values. On the other hand, the application of the considered approach to obtain preequilibrium α-spectra allows to reproduce the measured data.

2.1.3 Precompound deuteron emission

The calculations of deuteron precompound spectra were carried out with help of the exciton coalescence pick-up model combined with hybrid exciton model. The direct mechanism of deuteron emission was also taken into account.

The considered approach to obtain deuteron nonelastic spectra is briefly discussed below. The calculation of deuteron differential cross-sections in the framework of the coalescence pick-up model [8,9] without taking into account the direct processes shows the considerable discrepancy between calculated and experimental data. As an example, the calculated precompound spectrum of deuterons produced by irradiation of ^{54}Fe by 62 MeV-protons is presented in Fig.2. As seen from Fig.2 the obtained values differ noticeably from experimental data in high energy part of the spectrum. The variation of the model parameters, in particular the imaginary part of deuteron optical potential (W), does not enable to achieve the agreement between calculated and measured differential cross-sections, as follows from Fig.2. The similar conclusion has been made using the exciton model in a "closed" form in Ref.[9].

The reason of the divergence of calculated and experimental data is connected with the calculation of deuteron emission spectra without taking into account a direct mechanism of deuteron production which gives according to [10] the considerable contribution to differential cross-section for deuteron emission.

The contribution of the direct processes to deuteron emission can be taken into account using a phenomenological approach based on the hybrid exciton model. For this purpose let us consider the nucleon pick-up and deuteron emission from initial configuration (1p0h) [11,12]. The differential cross-section for nonequilibrium deuteron emission, formally, may be written in the following form

$$\frac{d\sigma^{pre}}{d\varepsilon_d} = \sigma_{non}\left\{\frac{\omega^*(E-Q_d-\varepsilon_d)}{\omega(1p,0h,E)}\cdot\frac{\lambda_c^d}{\lambda_c^d+\lambda_+^d}\cdot g_d + \right.$$
$$\left. +\sum_{n=3}\sum_{l+m=2} F_{l,m}(\varepsilon_d)\cdot\frac{\omega(p-1,h,E-Q_d-\varepsilon_d)}{\omega(p,h,E)}\cdot\frac{\lambda_c^d}{\lambda_c^d+\lambda_+^d}\cdot g_d\cdot D_n\right\} \qquad (11)$$

where $\omega^*(U)$ - is the density of excited states for nucleus formed after deuteron emission, g_d - is the single particle density for deuterons.

It should be noted that the second term in brackets of (11) describes the part of the nonequilibrium deuteron spectrum presented in Fig.2 and calculated in paper [9].

After emission of deuteron formed by nucleon pick-up from the configuration (p,h) the final state of the nucleus is (p-1,h+1). Therefore the density of final state may be written as

$$\omega^*(U) = \omega(0p,1h,U)\ \gamma/g_d\ , \qquad (12)$$

where γ - is a value characterizing the deuteron formation.

The comparison of the deuteron emission spectra calculated with the help of formula (11) and the measured spectra has made it possible to establish that the γ value shows the weak dependence from atomic mass number of target nucleus and may be considered as a constant with a good accuracy.

As an illustration the results of calculations of deuteron spectra with the γ value obtained from the experimental data are shown in Figs.3,4 for nuclei from C

to Au. For all nuclei the calculations have been performed using following values of parameters: $\gamma = 2 \cdot 10^{-3}$, and $\sum_{l+m=2} F_{l,m} = 0.3$. The imaginary part of deuteron optical potential was assumed to be equal to W = 16 MeV according Ref.[6]. The calculated deuteron spectra for 14.8 MeV-neutron induced reactions are shown in Fig.3 for iron, nickel, vanadium and copper isotopes. Due to the lack of experimental data for neutrons at the energies more than 20 MeV to verify the considered approach in the intermediate energy range the proton experimental data have been used. The deuteron spectra calculated for 62 MeV-proton induced reactions are shown in Fig.4 for various nuclei. Also the results of calculations for the incident 90 MeV-protons are presented. Contributions of the direct processes, the precompound processes corresponding to the $F_{1,1}$ and $F_{2,0}$ components and the equilibrium emission are shown in Figs.3,4. As seen from the figures only the consideration of all mentioned contributions allows to reproduce the measured deuteron spectra.

2.1.4 Equilibrium particle emission

The calculations of equilibrium particle spectra were performed on the basis of Weisskopf model. The emission of neutrons, protons, deuterons and α-particles was taken into account.

2.1.5 Nuclear level density

The nuclear level density was calculated with the help of the phenomenological approach [13] based on the generalised superfluid model for all nuclei formed in evaporation cascade.

The level density in generalised nuclear model can be described if we subdivide the excited states into quasiparticle, coherent and collective ones. Then the expression for nuclear level density is presented as

$$\rho(U)=\rho_{qp}(U')\cdot K_{vib}(U')\cdot K_{rot}(U'), \qquad (13)$$

where $\rho_{qp}(U')$ - is the density of quasiparticle (non-collective) nuclear excitations, $K_{vib}(U')$ and $K_{rot}(U')$ - are coefficients of level density enhancement due to vibrational and rotational states at the effective excitation energy U'.

Energy dependence of the quasiparticle level density has been calculated on the basis of superfluid nuclear model [14]. The correlation function for the ground states of nuclei was defined as Δ_0 = 12.0/A MeV. This choice of Δ_0 is consistent with the systematic of nuclear masses [15] and with the results of analysis of the experimental data on neutron resonances for heavy nuclei [14]. The critical temperature of the phase transition from superfluid to normal state, the condensation energy, the critical energy of the phase transition and the effective excitation energy are connected with correlation function Δ_0 by the following relations:

$$t_{cr}= 0.567\ \Delta_0$$

$$U_{cr}= 0.472a_{cr}\Delta_0^2- n\Delta_0 \qquad (14)$$

$$E_{con}= 0.152a_{cr}\Delta_0^2 - n\Delta_0\ ,$$

$$U'= U + n\Delta_0 + \delta_{shift},$$

where n=0, 1 and 2 for even-even, odd and odd-odd nuclei, correspondingly, and the empirical value of the excitation energy shift δ_{shift} was chosen on the base of consistent description of the density of low-lying collective levels and the data on neutron resonances.

The shell effects were included into consideration using the energy dependence of nuclear level density parameter a(U,A) obtained phenomenologicaly

$$a(U,Z,A) = \tilde{a}(A)\cdot\left(1+\delta W(Z,A)\cdot\frac{\varphi(U'-E_{cond})}{U'-E_{cond}}\right), \quad \text{for } U'> U_{cr}$$
$$a(U,Z,A) = a(U_{cr},Z,A), \quad \text{for } U' < U_{cr} \qquad (15)$$

where the asymptotic value of level density parameter at high excitation energy is equal to

$$\tilde{a}(A) = 0.073A + 0.115A^{2/3} \qquad (16)$$

where $\delta W(Z,A)$ is the shell correction to nuclear binding energy defined from the experimental values of nuclear masses or in the case of their lack with the help of the Mayers-Swiatecki formula [16], $\varphi(U)=\{1-\exp(-\gamma U)\}$ - is the dimensionless function which defines the energy dependence of the level density parameter at low excitation energies, value $\gamma=0.4A^{-1/3}$ was chosen from the description of density of neutron resonances.

The vibrational enhancement of nuclear level density was presented in the following form

$$K_{vib} = \exp\{\delta S-(\delta U/t)\}, \qquad (17)$$

where δS, δU are the difference of entropy and excitation energy connected with collective excitation modes and defined from relations for Bose-particle gas

$$\delta S = \sum_{i=1}^{\infty}(2\lambda_i+1)\{(1+n_i)\ln(1+n_i)-n_i\ln(n_i)\}$$
$$\delta U = \sum_{i=1}^{\infty}(2\lambda_i+1)\omega_i n_i, \qquad (18)$$

where ω_i and λ_i - are the energy and the multipolarity of collective excited state, n_i - is it population for given temperature. The attenuation of vibrational enhancement of

level density at high temperatures is taken into account by the following expression for level population

$$n_i = \frac{\exp\{-\gamma_i/(2\omega_i)\}}{\exp\{\omega_i/t\}-1} \qquad (19)$$

with the help of parameter γ_i obtained empirically on consistent description of the low-lying levels and the data on neutron resonances

$$\gamma_i = 0.0075A^{1/3}(\omega_i^2 + 4\pi^2t^2) \qquad (20)$$

Only quadrupole and octupole states were considered in the calculations. The position of the lowest state for all nuclei, with exception of ^{208}Pb, was defined by phenomenological expressions which well reproduce the experimental data

$$\omega_2 = 30A^{-1/3}\ ;\ \omega_3 = 50A^{-1/3} \qquad (21)$$

For nucleus ^{208}Pb the position of 2^+ state was assumed to be equal to experimental value 4.1 MeV.

For all spherical nuclei only coefficient of vibrational enhancement of the level density $K_{vib}(U')$ was taken into according to account in expression (11). For deformed nuclei the enhancement of level density connected with rotational mode of collective excitation $K_{rot}(U')$ was taken into account according to Ref.[14]

$$K_{rot}(U) = \sigma_\perp^2 g(U) = \sigma^2(1+\beta/3)g(U), \qquad (22)$$

where σ - is the spin cut-off factor, and $g(U)$ is the empirical function taking into account the attenuation of rotation modes at high energies proposed in Ref.[17]

$$g(U) = \{1 + \exp[(U-U_r)/d_r]\}^{-1}, \qquad (23)$$

where the parameters of attenuation function are connected with the parameter of quadrupole nuclear deformation β by relations:

$$U_r = 120A^{1/3}\beta^2\ ;\ d_r = 1400A^{-2/3}\beta^2 \qquad (24)$$

The parameter of quadrupole deformation was defined from formulae for nuclear masses [15].

The advantage of considered approach to obtain nuclear level density consists in calculation of cross-sections for magic and neighbouring nuclei taking into account shell effects. As an example Fig.5 presents the cross-sections for (p,2n2p), (p,3n2p), (p,4n2p) and (p,6n4p) for ^{90}Zr calculated provided the superfluid model and Fermi gas model with a=A/9.0 were used to calculate the nuclear level density. As seen from the Figure, the better agreement with experimental data in the whole energy range 0-100 MeV is observed in the case of level density calculation based on the superfluid model.

2.1.6 Equilibrium γ-ray emission

The probability of photon emission has been calculated through the following formula

$$\Gamma_\gamma(E)=\frac{1}{\pi\hbar^2c^2\rho(E)}\cdot\int\varepsilon_\gamma^2\sigma_\gamma(E-\varepsilon_\gamma)\rho(E-\varepsilon_\gamma)d\varepsilon_\gamma, \qquad (25)$$

where σ_γ is the photon absorption cross-section, ρ - is the nuclear level density.

The photon absorption cross-section has been obtained using the Lorentz formula

$$\sigma_\gamma(\varepsilon_\gamma)=\sum_{k=1}^{2}\frac{\sigma_k\varepsilon_\gamma^2\Gamma_{k\gamma}^2}{(\varepsilon_\gamma^2-E_{k\gamma}^2)^2+\varepsilon_\gamma^2\Gamma_{k\gamma}^2}, \qquad (26)$$

taking into account the splitting of dipole giant resonance in deformed nuclei. The position of maximum of dipole giant resonance taking into account the quadrupole nucleus deformation β was calculated in the following way [18]

$$E_{1\gamma}=E_0\,(1-\beta/3)^2;\ E_{2\gamma}=E_0\,(1-0.16\beta);\ E_0=43.4A^{-0.215} \qquad (27)$$

The widths of the resonances equal

$$\Gamma_1 = 0.232E_1;\ \Gamma_2 = 0.275E_2\ , \tag{28}$$

and the maximum value of photon absorption cross-section equals

$$\sigma_{1\gamma} = 145A/E_1;\ \sigma_{2\gamma} = 235A/E_2 \tag{29}$$

The nuclear level density for γ-channel has been calculated on the basis of the superfluid model consistently with other reaction channels.

The importance of taking into account γ-ray emission for some reactions induced by medium energy protons on neutron deficient nucleus in particular ^{124}Xe has been noted [19]. The taking into account the competition of γ-rays and particle emission permits to avoid sharp spurious peak near threshold in the calculation results for ^{124}Xe(p,np)^{123}Xe and for ^{126}Xe(p,np)^{125}Xe and ^{126}Xe(p,2np)^{124}Xe Fig.4. (upper part). Solid curves are the results obtained with γ-ray emission competition and dashed - without one. The experimental data for proton induced reaction for ^{124}Xe was taken from ref.[27,28,29] and for ^{126}Xe from ref. [30]. The taking into account γ-ray emission shifts effective reaction thresholds. In many cases the competition from γ-ray emission leads to some diminishing of cross section only, without essential change of excitation function energy dependence. Fig. 4 (lower part) shows the excitation functions for the neutron induced reactions on ^{93}Mo. The experimental data was taken from EXFOR for ^{95}Mo. The calculations with ALICE-92 code using consistent level density parameters in gamma and particle channels can be considered as a reasonable cross section evaluation.

2.1.7 Calculation of total reaction cross-sections and inverse reaction cross-sections

The calculation of reaction cross-sections were performed with the help of the optical model. The parameters of optical potentials are presented in Table 1 for neutrons, protons, alpha and deuterons.

Table 1

Optical model parameters for different incoming particles.

Parameter	Neutrons	Protons	Deuterons	α-particles
Real potential V (MeV)	48.0	60.0	$79.0+2Z/A^{1/3}$	50.2
Imagine potential W (MeV)	9.0	5.0	16.0	12.3
Form of W(r)	Surface	Volume	Surface.	Volume
Spin-orbit V_{so}(MeV)	7.0	7.5	5.6	0.001
Radius r_v (fm)	$1.151+1.77(A-2Z)/A^{4/3}$	1.2	1.15	$1.2+1.5/A^{1/3}$
r_w (fm)	r_v	1.55	1.01+1.26/A	r_v
r_{so} (fm)	r_v	1.25	0.98	1.00
Coulomb radii (fm)		1.25	1.30	1.30
Diffusivity a_v (fm)	0.66	0.60	0.81	0.564
a_w (fm)	0.64	0.50	0.68	0.564
a_{so} (fm)	0.64	0.51	1.00	1.000

2.1.8 Numerical calculations

The numerical calculations were carried out using modified ALICE-92 code. The principal changes in the code made by authors are briefly outlined below.

1. The calculation of the nuclear level density is performed in the framework of generalized superfluid model. The comparison of the calculated and experimental cross-sections at energies up to 100 MeV shows that the application of this model

results in a better agreement with the experimental data than using various modifications of Fermi-gas model.

2. The code allows to obtained the nonequilibrium spectra for the complex particles. The precompound α-particle spectra are calculated using the coalescence pick-up model [8] directly combined with the hybrid exciton model. The calculation of the deuteron nonequilibrium spectra is performed taking into account the direct processes on the basis of phenomenological approach described in Part 2.1.4. The test of the approaches used for the complex particle preequilibrium spectra calculation has been performed using available experimental data at the energies up to 100 MeV.

3. The inaccuracy in spectrum calculation for second emitted preequilibrium particle has been eliminated. The old algorithm [6] contained the inaccuracy connected with the calculation of two precompound particles contribution in the (n,np) or (p,np) reaction cross-section according to formula (7c) without the term $(1-V_p/\varepsilon)$. The absence of this term led in some cases to the incorrect cross-section description. (Example: the non-physical energy dependence of the calculated (n,2np) reaction cross-section for the uranium isotopes connected with the appearance of cross-section structure at low energies).

4. To obtain the total reaction cross-sections for incident neutrons and protons at energies above 100 MeV the data of Barashenkov [20] are used which obtained from the analysis of experimental data.

5. The parameters of the neutron optical potential have been corrected for heavy nuclei ($A > 230$) to achieve the agreement of calculated results with evaluated data from BROND-2, ENDF/B-VI, JENDL-3 and experimental data.

6. The inaccuracy in calculation of cross-sections taking into account γ-ray emission has been corrected. (It was connected with cross-section calculation for production of residual nuclei ${}_{Z}X^{A}$ with inaccurate consideration of contribution to this cross-section from photon emission for residual nucleus ${}_{Z}X^{A-1}$ or ${}_{Z-1}X^{A-1}$).

2.1.9 The examples of cross-section calculations

Cross-sections were calculated using global set of model parameters. In the case of discrepancy of calculated and experimental data at energies below 20 MeV the calculated values were corrected to achieve the agreement with the measured data.

To illustrate the typical deviation of experimental cross-sections from calculated values obtained using the global set of model parameters the Figs.7-13 show the results of calculation of neutron and proton induced reaction cross-sections for a number of reactions. As an examples the nuclei provided with the experimental data for (n,p), (n,α) and (n,2n) reactions have been selected. As seen from Figs.7-12 the shape of the calculated excitation functions agrees with the measured data. In some cases, the calculated cross-section values differ considerably from the experimental ones (example: ^{31}P). For these reactions the cross-sections values were corrected as described in part.2.2. Practically, there are no experimental neutron data at the energies up to 100 MeV. Therefore to illustrate the difference of the calculated and measured data at the energies more than 20 MeV the experimental proton induced reaction cross-sections have been used. The examples of such calculations are presented in Fig.13.

2.2 Semi-empirical cross-section evaluation

The calculated cross-section values were corrected using available experimental data and cross-section systematics.

In most cases the calculated values were normalized to known cross-section values at 14.5 MeV.

The normalization was performed simultaneously for (n,p), (n,α), (n,2n) and (n,np) reactions. The data library EXFOR and compilation [21] were used for reactions (n,p), (n,α) and (n,2n). The cross-section values evaluated on the basis of experimental data and obtained with help of the systematic dependence on neutrons and protons numbers in nuclei at 14.5 MeV were taken from Refs.[22,23] for these reactions.

To obtain the (n,p) reaction cross-section at 14.5 MeV the following formula was used also:

$$\sigma_{n,p} = \pi r_0^2 (A^{1/3}+1)^2 \left\{ A^{1.1108} \left[1.0318S^2 - 0.7143S + 0.11722 \right]^3 + 0.4506 \exp\left(-217.82S^2 - 2.095S\right) \right\} \qquad (30)$$

where r_0 =1.3 fm, S = (N-Z+1)/A.

The formula (30) has been obtained on the basis of experimental data from Ref.[22]. It describes the contribution of preequilibrium (first term in shaped brackets) and equilibrium (second term) processes to (n,p) reaction cross-section at 14.5 MeV. As follows from Table 2 the formula (30) presents a best fit to the experimental data, giving the lowest value of χ^2:

Table 2

Fits to 156 experimental cross-sections [22] for (n,p) reaction at 14.5 MeV obtained with various formulas

Formula	$\sum(\sigma_i^{exp}-\sigma_i^{calc})^2/(\Delta\sigma_i^{exp})^2$	χ^2	Reference
(30)	441.71	2.96	present
Forrest	474.28	3.12	[22,24]
Bychkov et al.	588.68	3.87	[22,25]
Ait-Tahar	756.50	4.91	[26]

For the (n,np) reaction at energy 14.5 MeV the systematic obtained in Ref.[24] has been used as well as the cross-sections evaluated in this work on the basis of experimental data.

The examples of calculated cross-section correction are presented in Fig.14 for ^{56}Fe and ^{58}Ni. The cross-sections calculated for all cross-sections shown in Fig.14 were corrected according to the available experimental data.

3. MENDL data format

The data of MENDL library are presented in the ENDF-6 format. The files MF=1 and MF=3 are used for the data recording. File MF=1 contains the general description of the type of cross-sections presented and the file MF=3 includes the obtained cross-section values. The standard ENDF MT sections as well as the new assigned sections are used to record the information in file MF=3.

The detail description of the new assigned sections is given for each nuclide in the file MF=1.

3.1 MENDL catalogue

The MENDL catalogue includes the following information.

The line beginning with symbol "*" contains the characteristics of target nucleus with indication atomic number, name of element, atomic mass number, half-life and total number of reactions considered nucleus and contained in MENDL files.

The line with reaction description indicates:

a) Atomic number (Z), name of element and mass number (A) for target nucleus;
b) Reaction type; "(N,X)" symbols mean the sum of cross sections for all possible reactions resulting in the same residual nucleus without taking into account radioactive decay chains;
c) Z, name and A for nucleus produced;
d) Half-life of the product nucleus; Symbols "S", "M", "H", "D" and "Y" signify Second, Minute, Hour, Day and Year, correspondingly;
e) The number of energy points for which the cross-sections for given reaction are available in MENDL;
f) The minimum reaction energy (Q) in MeV for all reactions resulting in considered product nucleus;
g) The indication of the origin of cross sections presented.

EXAMPLE

```
13-Al-26 (N,X) 11-Na-22 2.60E+00Y 68 -9.450E+00 Original
```

Meaning

`13-Al-26` :	target nucleus is aluminum isotope with A=26
`(N,X)` :	sum of (n,nα) and (n,3n2p) reaction cross-sections
`11-Na-22` :	product nucleus is sodium isotope with A= 22
`2.60E+00Y` :	half-life of ^{22}Na is equal 2.6 year
`68` :	the number of energy points given for this reaction is equal to 68
`-9.450E+00` :	Q-value for (n,nα) reaction
`Original` :	reaction cross-section has been obtained by authors

Table 3.

CONTENT

Target			Half-life	Number of reactions		
*13-Al-26	unstable		7.205E+05 Y	74 reactions		
Target	Reaction	Product	Half-life	Points	Q-value	Comments
13-Al- 26	(N,2N)	13-Al- 25	7.18E+00S	67	-1.137E+01	Original
13-Al-26	(N,3N)	13-Al- 24	2.07E+00S	47	-2.830E+01	Original
13-Al-26	(N,4N)	13-Al- 23	4.70E-01S	31	-4.319E+01	Original
13-Al- 26	(N,5N)	13-Al- 22	7.00E-02S	18	-6.253E+01	Original
13-Al-26	(N,6N)	13-Al- 21	short	10	-7.813E+01	Original
13-Al- 26	(N,P)	12-Mg- 26	stable	90	4.786E+00	Original
13-Al- 26	(N,X)	12-Mg- 25	stable	81	-4.082E+00	Original
13-Al- 26	(N,X)	12-Mg- 24	stable	65	-1.141E+01	Original
13-Al- 26	(N,X)	12-Mg- 23	1.13E+01S	46	-2.794E+01	Original
13-Al- 26	(N,X)	12-Mg- 22	3.86E+01S	32	-4.109E+01	Original
13-Al- 26	(N,X)	12-Mg- 21	1.23E-01S	19	-6.047E+01	Original
13-Al- 26	(N,X)	12-Mg- 20	9.50E-02S	11	-7.419E+01	Original
13-Al- 26	(N,2P)	11-Na- 25	5.96E+01S	70	-9.358E+00	Original
13-Al- 26	(N,X)	11-Na- 24	1.50E+01H	58	-1.614E+01	Original
13-Al- 26	(N,X)	11-Na- 23	stable	90	2.968E+00	Original
13-Al- 26	(N,X)	11-Na- 22	2.60E+00Y	68	-9.450E+00	Original
13-Al- 26	(N,X)	11-Na- 21	2.25E+01S	53	-2.052E+01	Original
13-Al- 26	(N,X)	11-Na- 20	4.46E-01S	35	-3.762E+01	Original
13-Al- 26	(N,X)	11-Na- 19	3.00E-02S	24	-5.178E+01	Original
13-Al- 26	(N,X)	11-Na- 18	short	12	-7.353E+01	Original
13-Al- 26	(N,X)	11-Na- 17	short	3	-9.166E+01	Original
13-Al- 26	(N,3P)	10-Ne- 24	3.38E+00M	53	-2.006E+01	Original
13-Al- 26	(N,X)	10-Ne- 23	3.72E+01S	46	-2.670E+01	Original
13-Al- 26	(N,X)	10-Ne- 22	stable	73	-5.826E+00	Original
13-Al- 26	(N,X)	10-Ne- 21	stable	59	-1.396E+01	Original
13-Al- 26	(N,X)	10-Ne- 20	stable	52	-2.072E+01	Original
13-Al- 26	(N,X)	10-Ne- 19	1.77E+01S	34	-3.759E+01	Original
13-Al- 26	(N,X)	10-Ne- 18	1.67E+00S	24	-4.923E+01	Original
13-Al- 26	(N,X)	10-Ne- 17	short	15	-6.846E+01	Original
13-Al- 26	(N,X)	10-Ne- 16	short	6	-8.611E+01	Original
13-Al- 26	(N,4P)	9- F- 23	short	34	-3.665E+01	Original
13-Al- 26	(N,X)	9- F- 22	4.23E+00S	29	-4.197E+01	Original
13-Al- 26	(N,X)	9- F- 21	4.32E+00S	50	-2.109E+01	Original
13-Al- 26	(N,X)	9- F- 20	1.10E+01S	45	-2.697E+01	Original
13-Al- 26	(N,X)	9- F- 19	stable	68	-7.501E+00	Original

REFERENCES

1. Mann F.M. Transmutation of Alloys in the MFE Facilities as Calculated by REAC (A Computer System for Activation and Transmutation) /HEDL-TME,81-37, (1982).

2. Kopecky J., Nierop D., Contents of EAF-2. ECN-1-91-053, (1991).

3. Грудзевич О.Т., и др., Каталог библиотеки ADL-3., *Вопросы атомной науки и техики. Сер. Ядерные константы.*, (1993), выпуск 3-4.

4. Конобеев А.Ю., и др., Библиотека сечений для изучения процесса трансмутации и активации материалов, облучаемых нейтронами и протонами с энергией до 100 МэВ., *Вопросы атомной науки и техники. Сер. Ядерные константы.*, (1992), выпуск 3-4., стр. 55.

   Shubin Yu.N., et al., MENDL Activation Data Library for Intermediate Energies. Report IAEA-NDS-136, Rev. 0, May 1994.

5. Blann M., Importance of the Nuclear Density Distribution on Pre-Equilibrium Decay., *Phys. Rev. Lett.*, **v.28** (1972) 757.

6. Blann M., Vonach H.K., Global Test of Modified Precompound Decay Models., *Phys. Rev.* **v.C28** (1983) 1475.

7. Kikuchi K., Kawai M., Nuclear Matter and Nuclear Interactions North-Holland, Amsterdam, (1968).

8. Iwamoto A.,Harada K., Mechanism of Cluster Emission in Nucleon-Induced Preequilibrium Reactions., *Phys. Rev.* **v.C26** (1982) 1821.

9. Sato N., Iwamoto A., Harada K., Preequilibrium Emission of Light Composit Particles in the Framework of the Exciton Model., *Phys. Rev.* **v.C28** (1983) 1527.

10. Gadioli E., Emission of complex particles in precompound reactions., Report of Instituto Nazionale di Fisica Nucleare., (1988) Milano, Italy, INFN/BE-88-2.

11. Dobes J., Betak E., Proc. Int. Conf. React. Models 77, Balatonfured, (1977), p.195.

12. Kalbach C., The Griffin Model, Comlex particles and Direct NuclearReactions., *Z.Physik,* **v.A283** (1977), p. 401

13. Игнатюк А.В., Вклад коллективных движений в плотность возбужденных состояний ядра., *Ядерная физика* **т. 21,**(1975) 20

Блохин А.И., Игнатюк А.В., и др., Анализ функций возбуждения пороговых реакций в обобщенной сверхтекучей модели., *Известия Академии наук СССР Сер. физическая* **т. 49,**(1985) 962

Блохин А.И., Игнатюк А.В., Шубин Ю.Н., Вибрационное увеличение плотности уровней ядер области железа., *Ядерная физика* **т.48,**(1988) 371

Ignatyuk A.V., et al., Density of Discrete Levels in ^{116}Sn., *Phys. Rev.* **v.C47** (1993) 1504.

14. Игнатюк А.В., Истеков К.К., Смиренкин Г.Н., Роль коллективных эффектов при систематике плотности уровней ядер., *Ядерная физика* **т. 29,**(1979) 875

15. Myers W.D., Droplet Model of Atomic Nuclei, IFI/Plenum Press N.Y., 1977

16. Mayers W.D. and Swiatecki W.J., Anomalies in Nuclear Masses., *Arkiv for Fysik* **v.36** (1967) 343.

17. Hansen G. and Jensen A.S., Energy dependence of the rotational enchancement factor in the level density., *Nucl.Phys.,* **v.A406** (1983) 236

18. Blann M., Reffo G., Fabbri F., Calculation of γ-ray Cascades in Code ALICE., *Proc. Meeting on Methods for the Calculations of Neutron Nuclear Data.* Bologna, Italy, 1986, p.107

19. Shubin Yu.N., Rep. in *IAEA Advisory Group Meeting on Intermediate Energy Nuclear Data for Applications*, Vinna (1990)

Lunev V.P., et al., An Analysis of Reaction cross section Calculation Methods for the Production of Medical Radioisotopes. in *Proc. Int. Conference on Nuclear Data for Science and Technology.* Julich (1991) p.609.

Blann M., et al., Effect of Gamma Emission Competition on the Excitation Function Description for the Reactions Induced by Medium Energy Nucleons. in *Proc. Int. Conference on Nuclear Data for Science and Technology.* Gatlinburg (1994).

20. Барашенков В.С. Нуклон-ядерные сечения., Препринт ОИЯИ, Дубна, 1989, Р2-89-770

21. Бычков В.М., Манохин В.Н., Пащенко А.Б., Пляскин В.И. Сечения пороговых реакций, вызываемых нейтронами. Справочник. Москва, Энергоиздат, 1982.

Bychkov V.M., Manokhin V.N., Pashchenko A.B., Plyaskin V.I., Cross-section for neutron induced threshold reactions, (in russian) Moscow, Energoatomizdat, 1982.

22. Badikov S.A., Pashchenko A.B., Comparative analysis of (n,p) reaction cross-section systematics at neutron energy 14-15 MeV, Preprint of Institute of Physics and Power Engineering, N 2055, Obninsk, 1989.

23. Pashchenko A.B., Cross-Sections for Reaction Induced by 14.5 MeV Neutrons and by Neutrons of Cf-252 and U-235 Fission spectra., Preprint N0236, Moscow, TSNIIAtominform, 1990.

24. Forrest R.A., Systematics of Neutron-Induced Threshold Reactions with Charged Products at about 14.5 MeV, AERE-R12149, Harwell Laboratory, 1986.

25. Bychkov V.M., Pashchenko A.B., Plyaskin V.I., Interpretation of (N-Z) dependence for (n,p) reaction cross-section at energy 14-15 MeV, Preprint of Institute of Physics and Power Engineering, N 809, Obninsk, 1978.

26. Ait-Tahar S., The systematics of (n,p) cross-sections for 14 MeV neutrons, *J. Phys. G: Nucl.Phys.* **v.13** (1987) L121.

27. Kurenkov N.V. et al., Excitation functions of proton-induced nuclear reactions on ^{124}Xe: Production of ^{123}I. *J.Radioanal.Nucl.Chem.Lett.* **v.135**, (1989) p.39.

28. Tàrkànyi F. et al., Excitation Function of (p,2n) and (p,pn) Reactions and Differential and Integral Yeilds of ^{123}I in Proton Induced Nuclear Reactions on Highly Enriched ^{124}Xe. *Appl. Rad.Isot.* **v.42**,(1991), p.221.

29. Tàrkànyi F. et al., Nuclear Reaction Cross Section Relevant to the Production of the ^{122}Xe-^{122}I Generator System using Highly Enriched ^{124}Xe and a Medium-sized Cyclotron. *Appl. Rad.Isot.* **v.42**,(1991), p.229.

30. Venikov N.I. et al., Excitation functions of proton-induced reactions on ^{126}Xe: ^{125}I Impurity in ^{123}I. *Appl. Rad.Isot.* **v.44**,(1993), p.51.

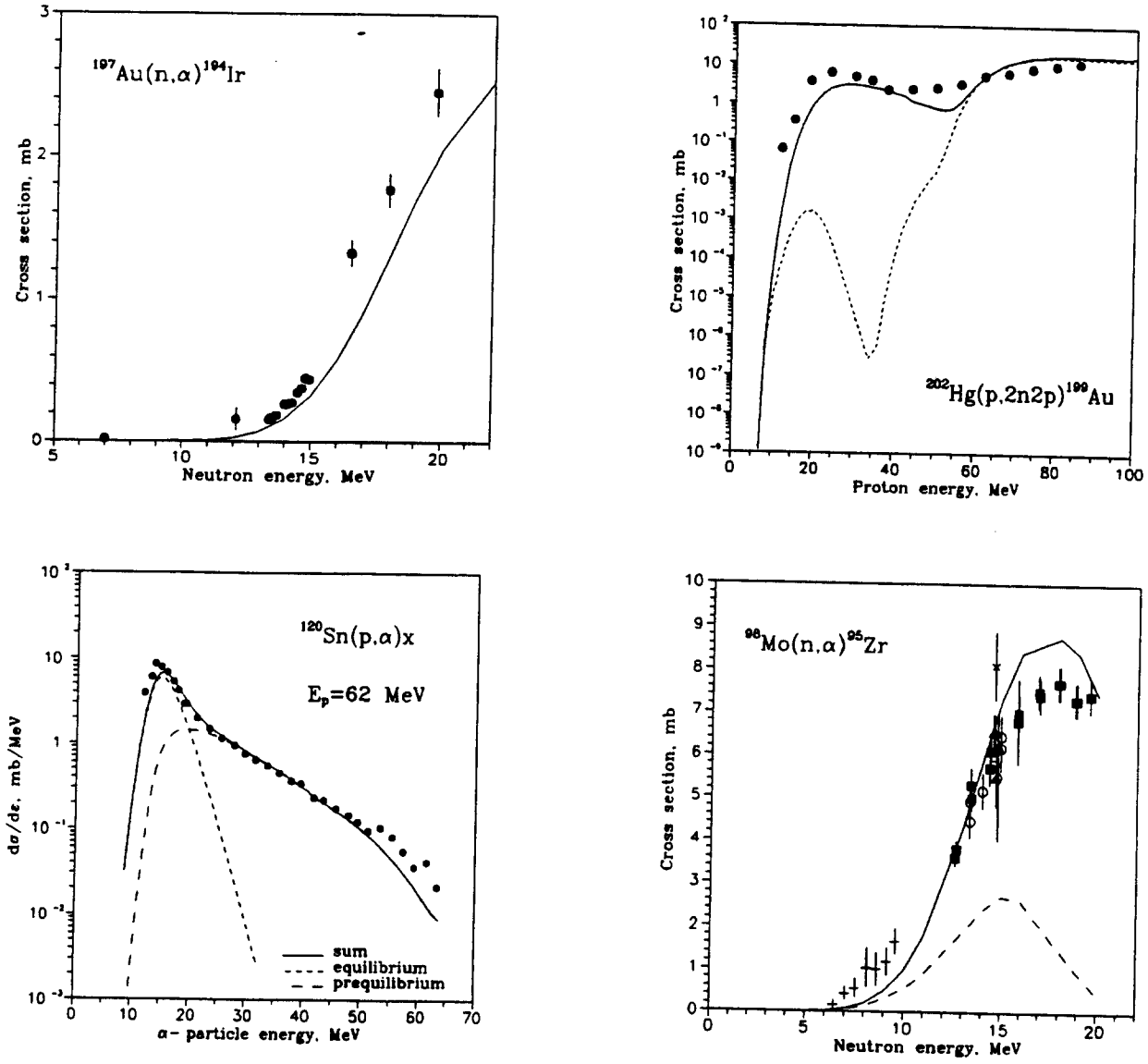

Fig. 1. Preequilibrium α-emission prediction and experimental data for proton and neutron induced reactions. For ^{197}Au(n,α) reaction solid line represents sum of equilibrium and preequilibrium processes. For ^{202}Hg(p,2p 2n)^{197}Au reaction short dashed line - contribution from equilibrium processes. For ^{98}Mo(n,α)^{95}Zr reaction dashed line - contribution from equilibrium processes. For ^{120}Sn(p,α) reaction α-particles spectrum is introduced (long dashed curve - represents preequilibrium α-particles emission, solid line - sum of equilibrium and preequilibrium processes). Difference between curves is due to preequilibrium α-emission.

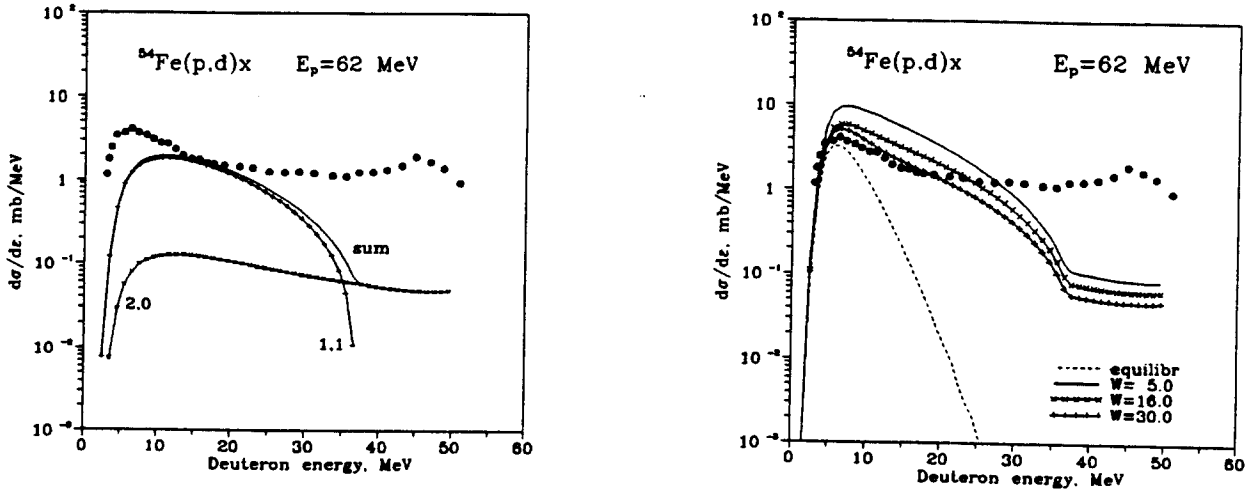

Fig. 2. Deuteron emission spectra calculated without taking into account the direct processes. The left figure presents the precompound deuteron spectrum as well as the $F_{1,1}$ and $F_{2,0}$ [9] contribution components. The right figure shows the total deuteron spectrum obtained provided the precompound calculations have been performed using different values of the deuteron optical potential imaginary part W.

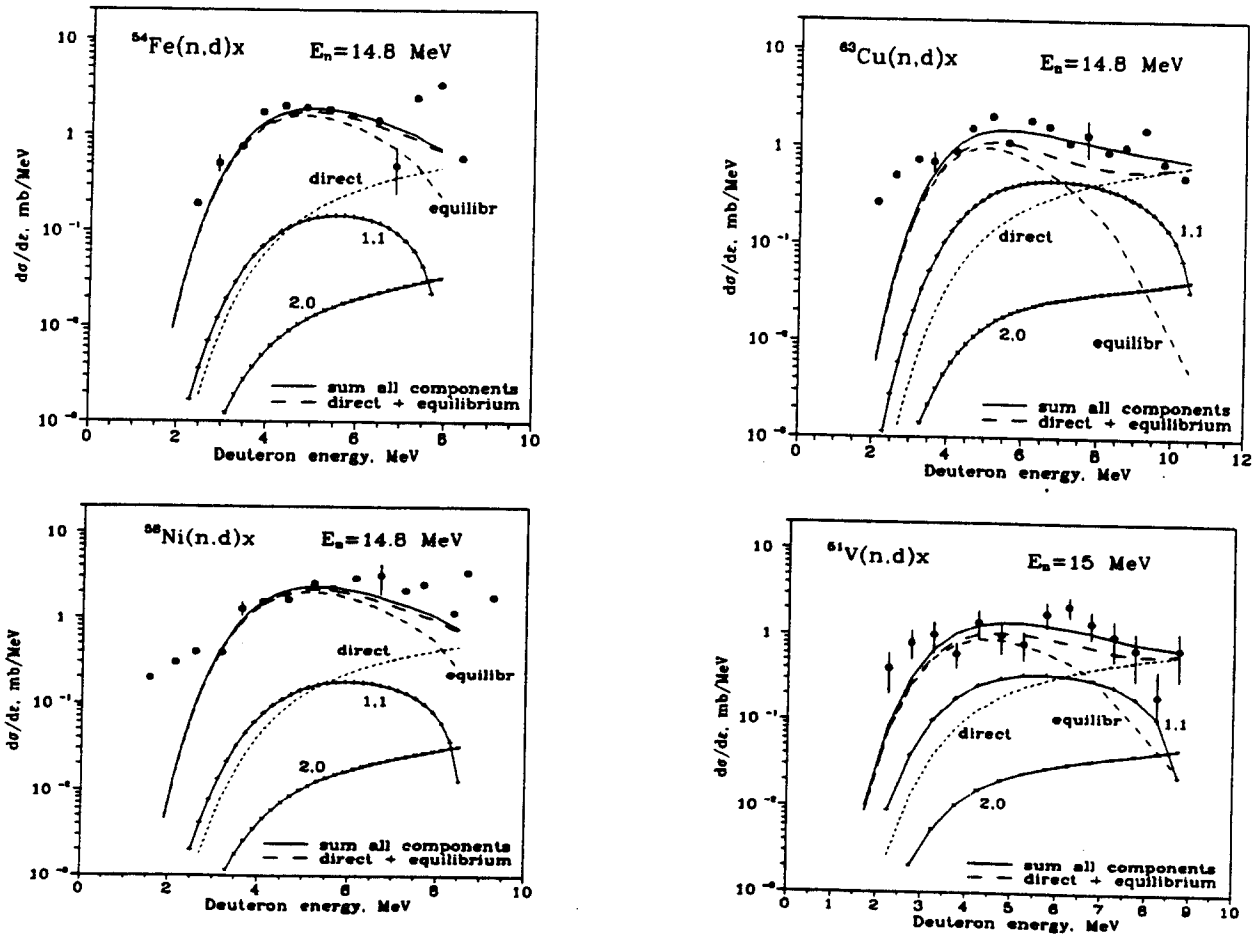

Fig. 3. Calculated deuteron emission spectra for 14.8 MeV incident neutron induced reactions. The contributions of the direct processes, $F_{1,1}$ and $F_{2,0}$ precompound and equilibrium processes are shown.

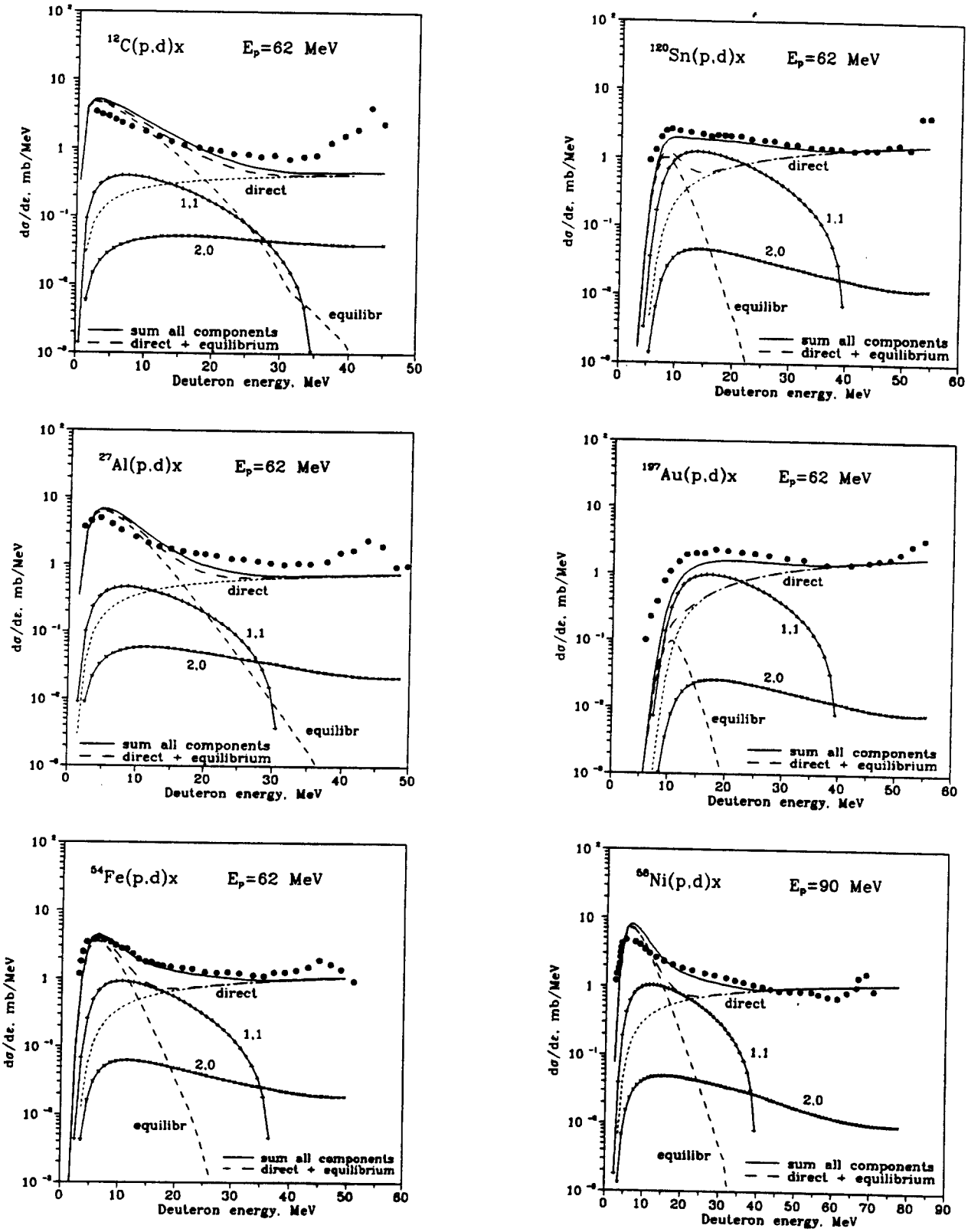

Fig. 4. Calculated deuteron emission spectra for intermediate energy proton induced reactions. The contributions of different processes to the emission spectra are shown..

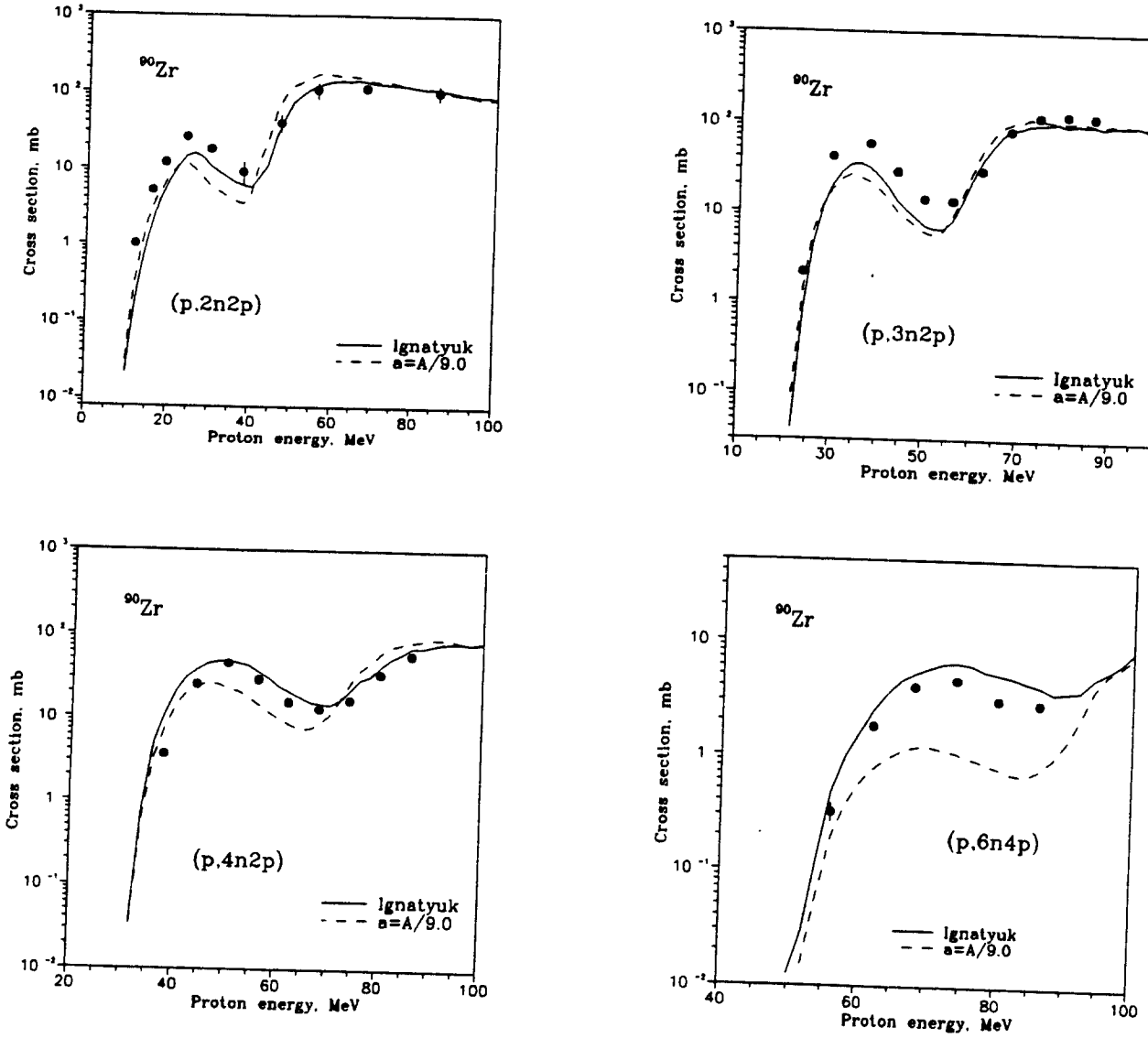

Fig. 5. Effect of different models for level density calculations. Dashed line - calculations with Fermi-gas model (a=A/9.) and solid line - superfluid model.

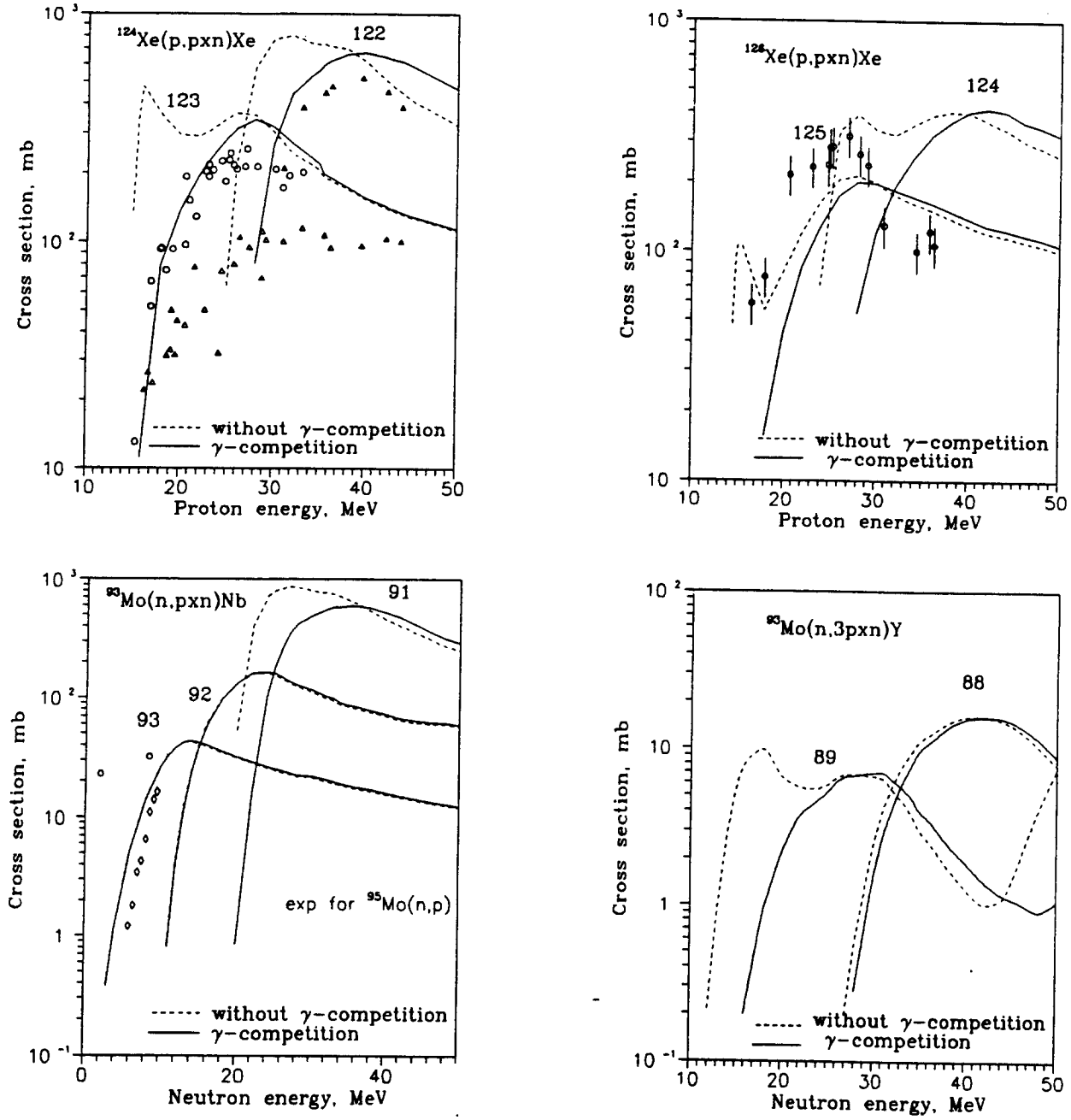

Fig. 6. Effect of gamma competition on excitation functions for proton induced (^{124}Xe(p,pxn)Xe and ^{126}Xe(p,pxn)Xe (upper part of figure)) and for neutron induced (^{93}Mo(n,pxn)Nb, ^{93}Mo(n,3p2n)^{89}Y and ^{93}Mo(n,3p3n)^{88}Y (lower part)) reactions.

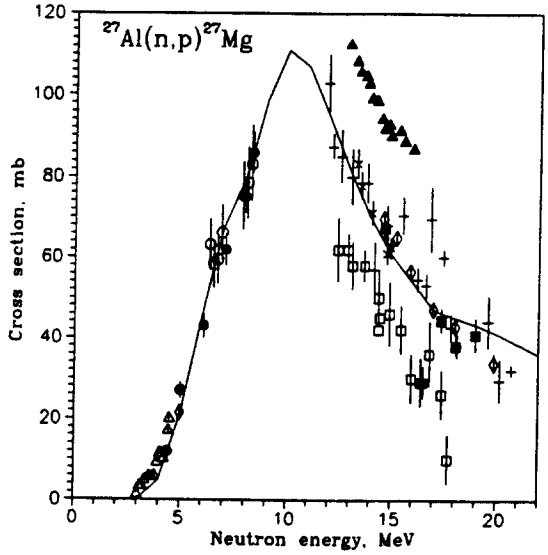

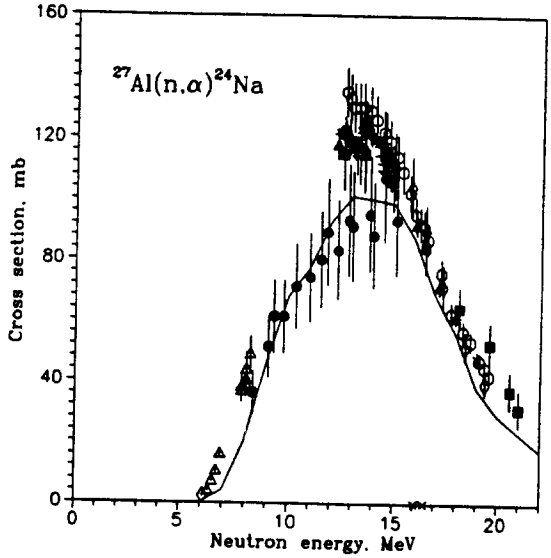

Fig. 7. Neutron induced reaction cross-sections for ^{27}Al calculated using the global set of model parameters for- ^{27}Al(n,p)^{27}Mg reaction (left) and -^{27}Al(n,α)^{24}Na reaction (right).

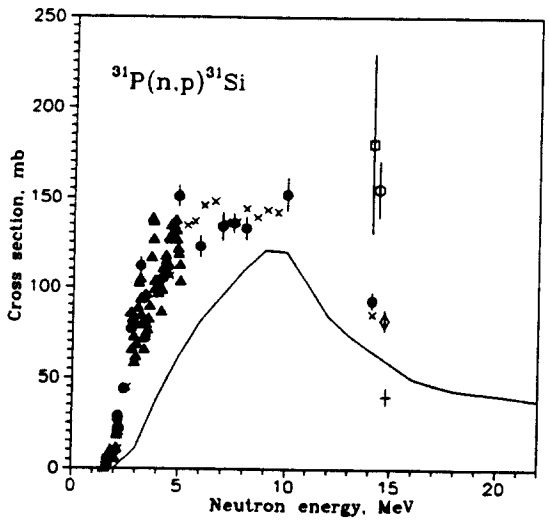

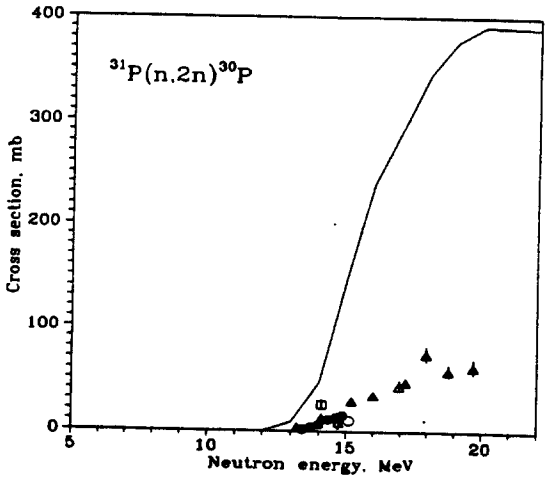

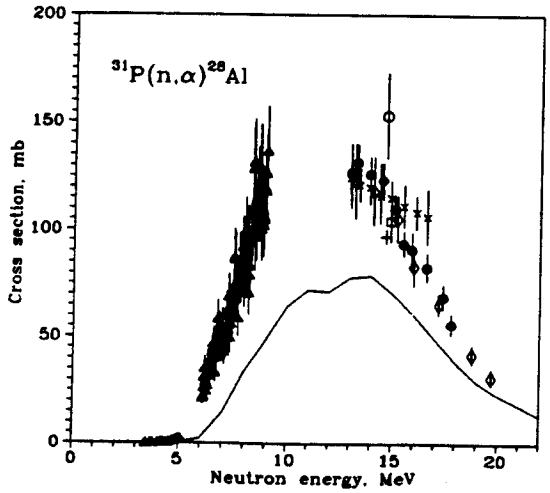

Fig. 8. Neutron induced reaction cross-sections calculated using the global set of model parameters for ^{31}P.

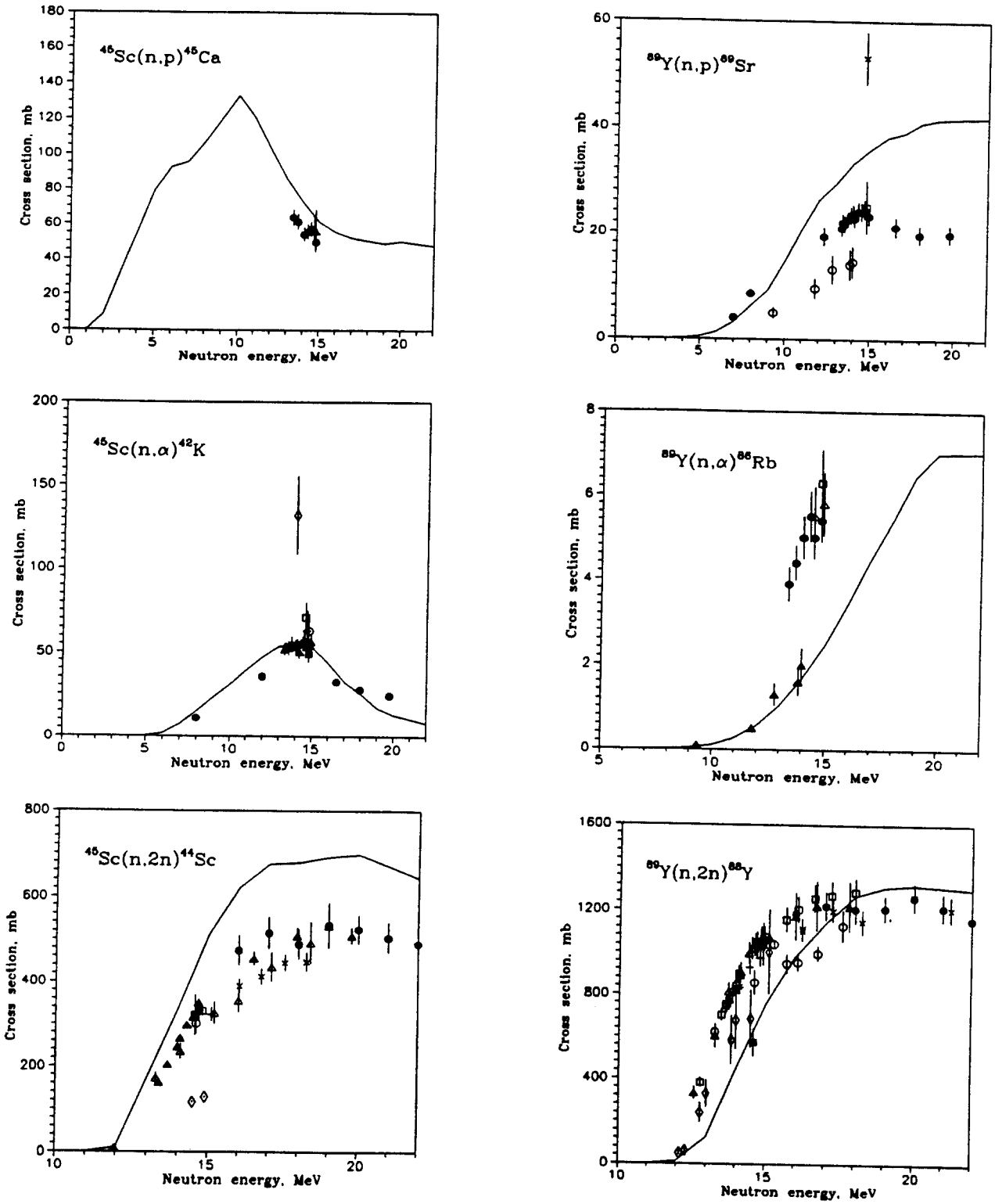

Fig. 9. Neutron induced reaction cross-sections calculated using the global set of model parameters for ^{45}Sc and ^{89}Y.

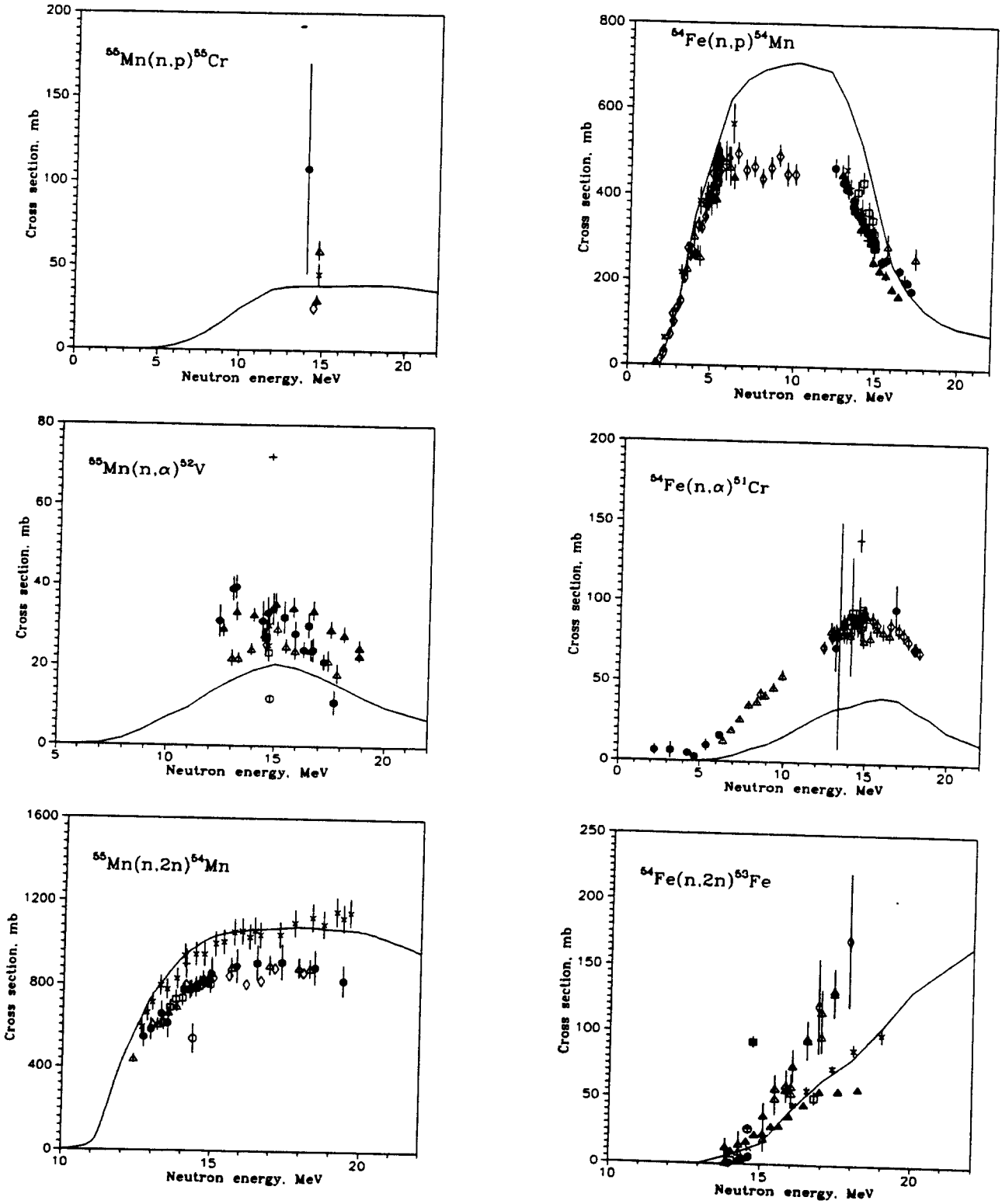

Fig. 10. Neutron induced reaction cross-sections calculated using the global set of model parameters for ^{55}Mn and ^{54}Fe

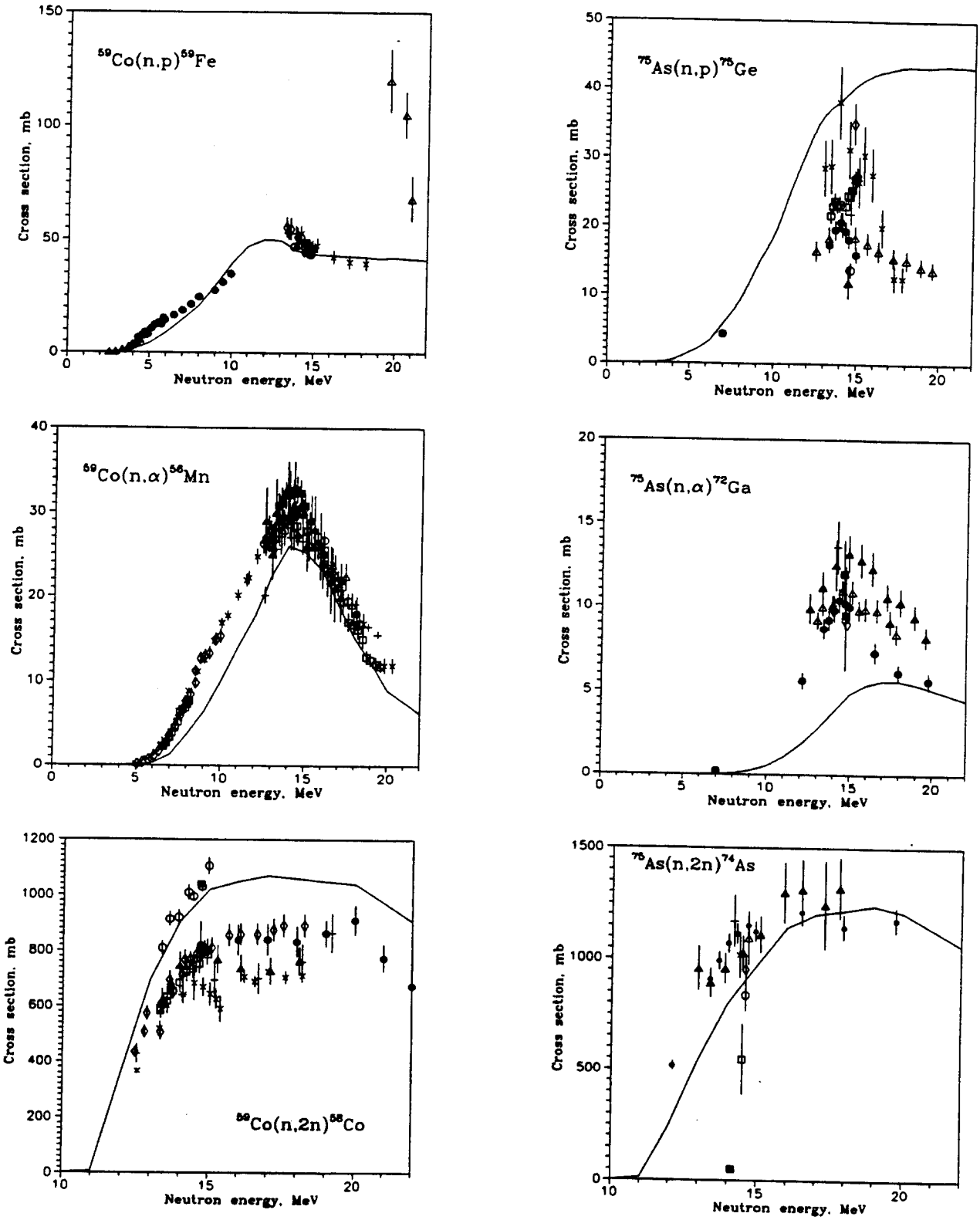

Fig. 11. Neutron induced reaction cross-sections calculated using the global set of model parameters for ^{59}Co and ^{75}As.

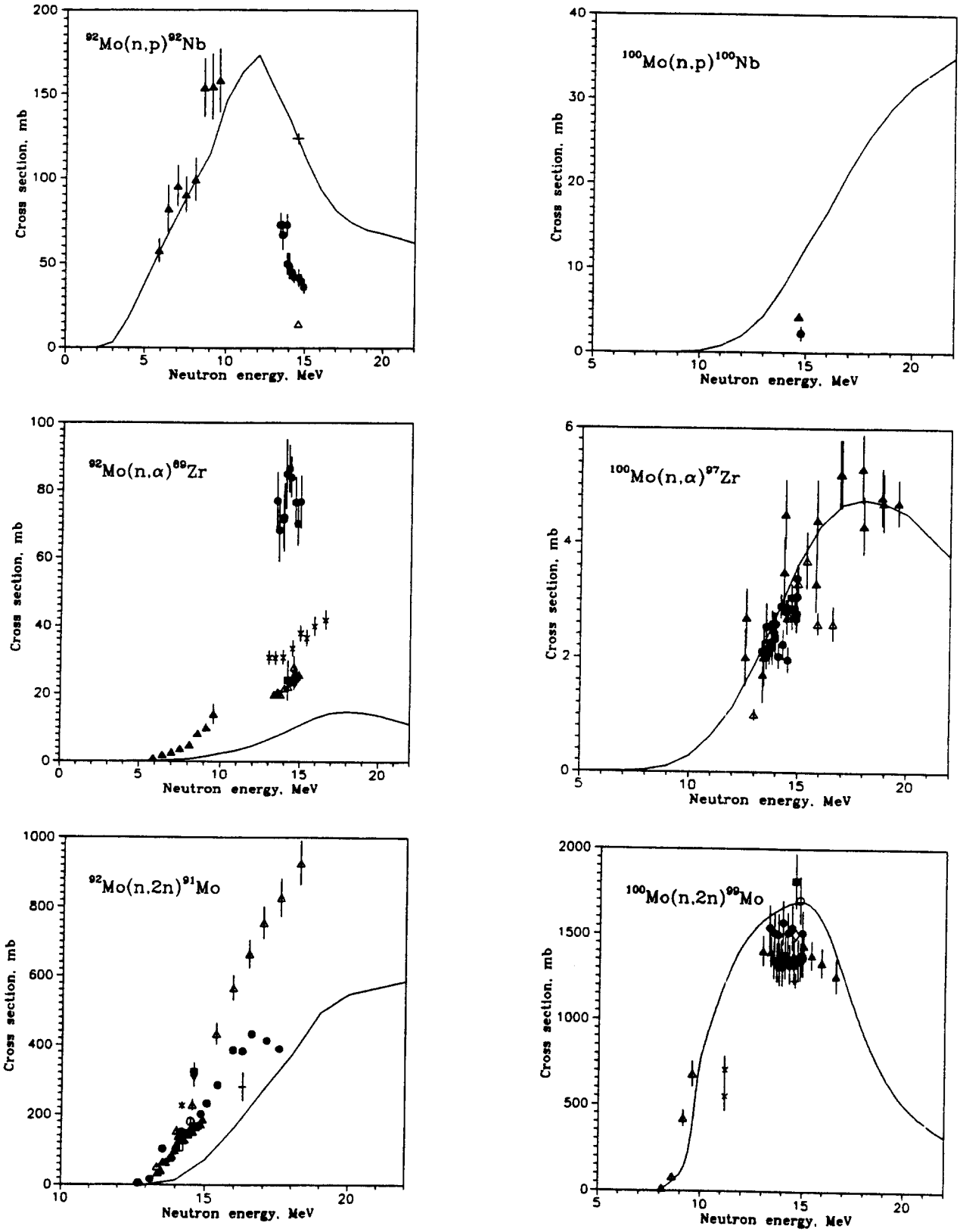

Fig. 12. Neutron induced reaction cross-sections calculated using the global set of model parameters for ^{92}Mo and ^{100}Mo. For ^{92}Mo(n,p) reaction the experimental data and the systematics value ("+") calculated according to the formula (30) are shown.

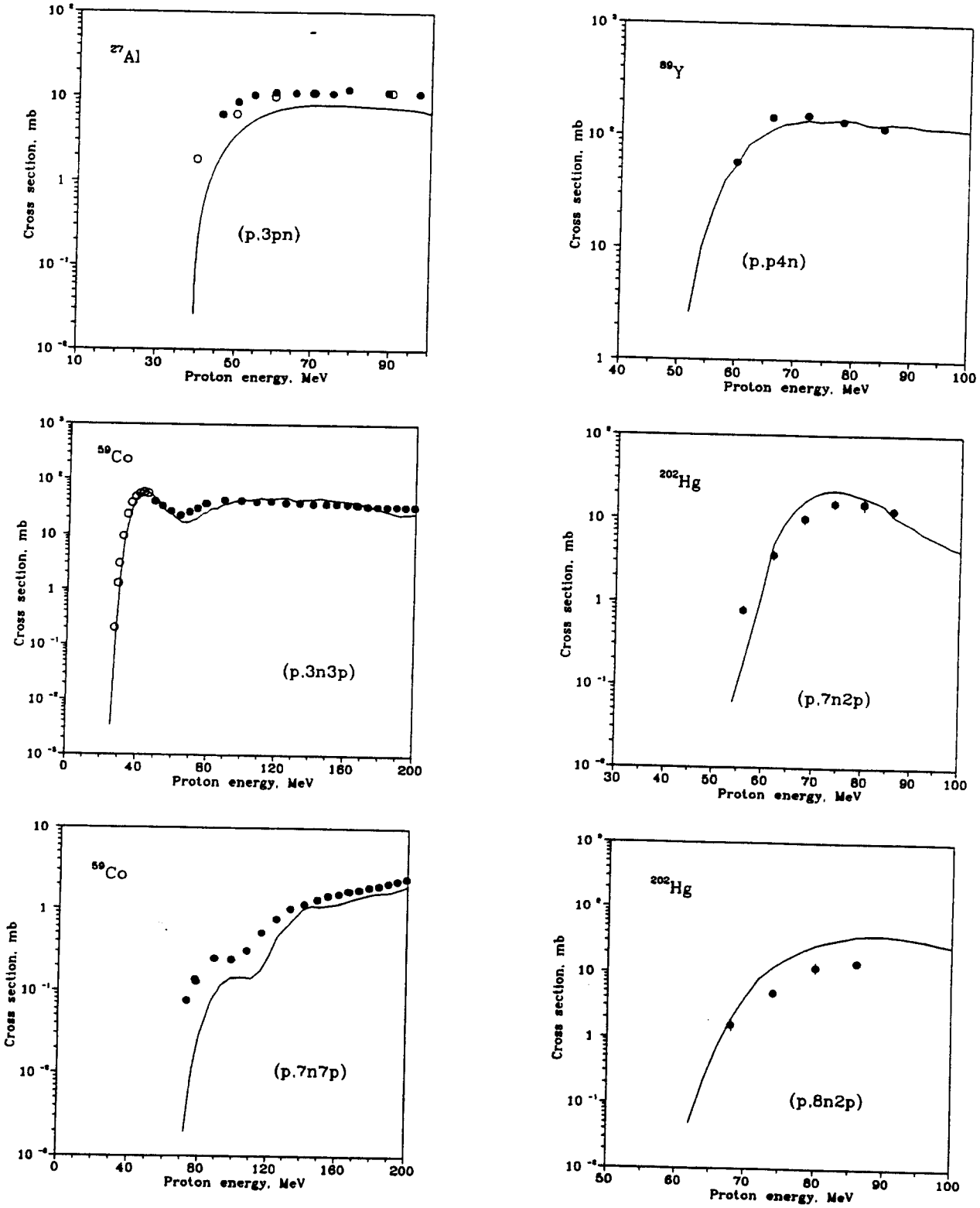

Fig. 13. Comparison of proton induced reaction cross-section calculated using the global set of model parameters with the intermediate energy proton experimental data

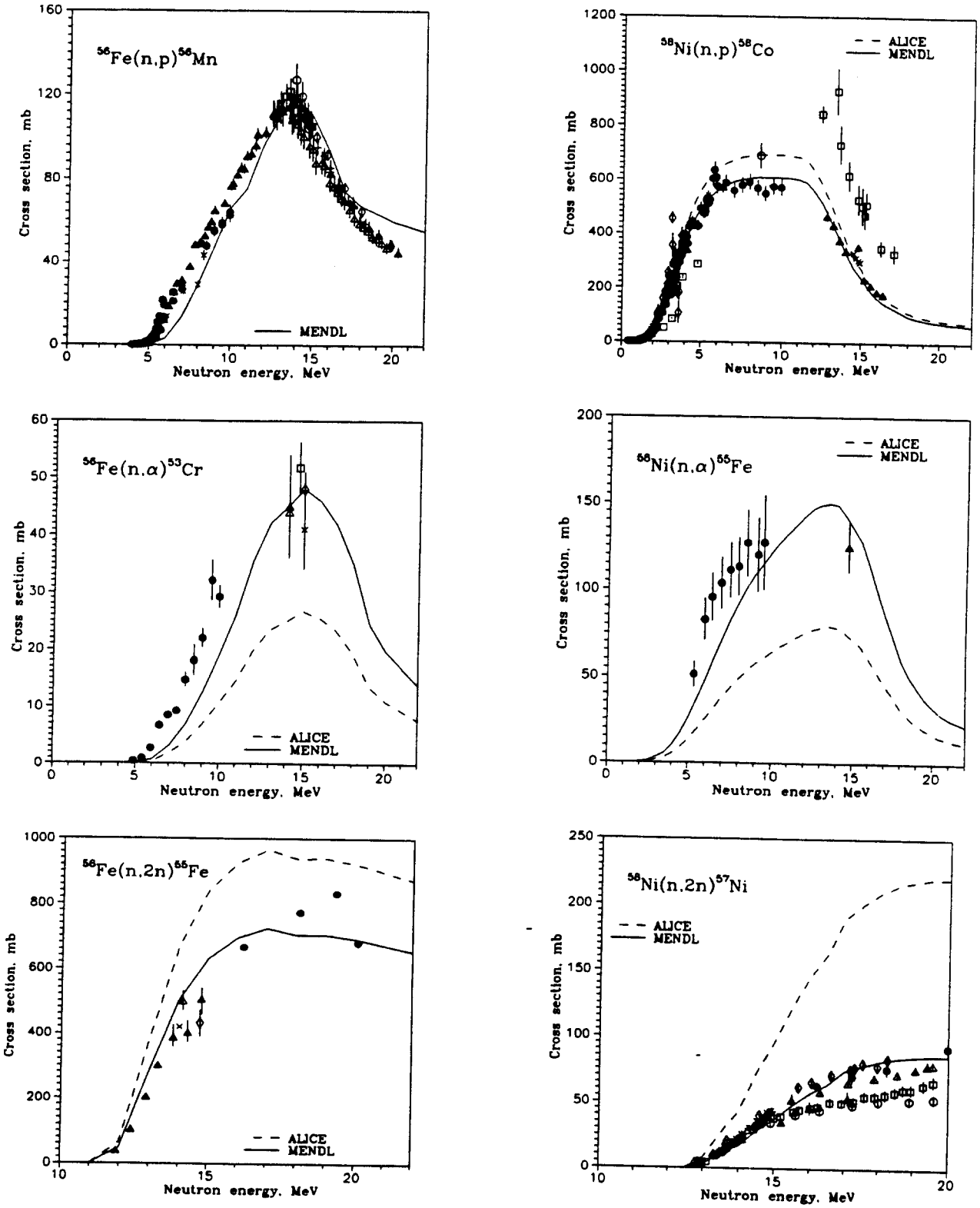

Fig. 14. Examples of the neutron induced excitation functions correction for (n,p), (n,α) and (n,2n) reactions on ^{56}Fe and ^{58}Ni experimental data.